INORGANIC CHEMISTRY FRONTIERS

RESEARCH ARTICLE

View Article Online
View Journal

Cite this: DOI: 10.1039/d5qi02376a

Latent one-dimensional luminescent coordination polymer emerging from copper(I) iodide secondary building units

Kazuma Kikuchi,[a] Shuji Nagata,[b] Takashi Yumura,[b] Takahiro Iwamoto,[a] Kensuke Naka[a,c] and Hiroaki Imoto[*a,c,d]

Received 22nd November 2025,
Accepted 5th February 2026

DOI: 10.1039/d5qi02376a

rsc.li/frontiers-inorganic

Luminescent coordination polymers (CPs) often exhibit poor processability and recyclability owing to their insoluble infinite networks. Herein, we report a reversible vapor-induced structural interconversion between a zero-dimensional (0D) complex and a one-dimensional (1D) luminescent CP, which enables both solution processing and recycling. The 1D CP $[Cu_2I_2(AsPh_3)_2(\mathbf{meprz})]_n$ (**Crys-B**) with intense yellow emission was converted to the weakly emissive 0D complex $Cu_2I_2(AsPh_3)_2(\mathbf{meprz})_2$ (**Crys-A**) upon exposure to 2-methylpyrazine (**meprz**) vapor, and reverted back to **Crys-B** upon exposure to acetonitrile (CH_3CN) vapor. This transformation proceeded smoothly without amorphization, allowing film fabrication *via* casting or spin-coating in the 0D state, followed by vapor-induced polymerization, while enabling recovery *via* depolymerization. Comparative studies revealed that the arsine ligand ($AsPh_3$) accelerates vapor-induced switching and enhances the emission contrast relative to its phosphine analog (PPh_3). This study established the first copper(I) halide-based luminescent CP to achieve reversible 0D/1D conversion, offering a practical route for processable and recyclable luminescent materials.

Introduction

Coordination polymers (CPs) tend to exhibit superior material properties compared with zero-dimensional (0D) complexes (Fig. 1a).[1] In particular, luminescent CPs often demonstrate higher emission efficiencies and enhanced thermal, chemical, and photostabilities relative to their 0D counterparts. For example, Hasegawa *et al.* developed highly efficient and thermally robust Eu(III) CPs using bisphosphine oxides as bridging ligands.[2] Despite these remarkable advantages, the inherently insoluble and infinite network structures of CPs result in poor processability and recyclability. Various strategies have been explored to improve their processability, including blending with polymer matrices,[3] hybridization with organic shells,[4] and chemical vapor deposition.[5] A conceptually simple and effective alternative involves solid-phase interconversion between the 0D and CP forms, enabling both the processability and recyclability of a single material (Fig. 1b). This concept involves three key steps: (1) processing the material in its soluble 0D form; (2) converting it into an extended CP form to

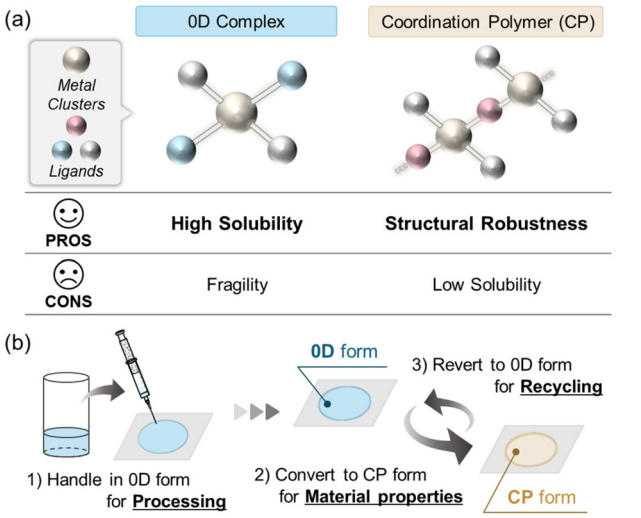

Fig. 1 (a) Comparison of the key features of 0D complexes and CPs. (b) Schematic illustration of reversible 0D–CP transformation for (1) processing, (2) usage, and (3) recycling.

[a]*Faculty of Molecular Chemistry and Engineering, Kyoto Institute of Technology, Gashokaido-cho, Matsugasaki, Sakyo-ku, Kyoto 606-8585, Japan. E-mail: himoto@kit.ac.jp*
[b]*Faculty of Material Science and Technology, Kyoto Institute of Technology, Goshokaido-cho, Matsugasaki, Sakyo-ku, Kyoto 606-0962, Japan*
[c]*Materials Innovation Lab, Kyoto Institute of Technology, Goshokaido-cho, Matsugasaki, Sakyo-ku, Kyoto 606-8585, Japan*
[d]*Fusion Oriented REsearch for disruptive Science and Technology (FOREST), Japan Science and Technology Agency (JST), Honcho 4-1-8, Kawaguchi, Saitama 332-0012, Japan*

leverage its superior material properties; and (3) reverting it to its original 0D form for recycling.

A common approach to the interconversion between the 0D and CP forms involves thermoresponsive structural changes. For instance, Julve *et al.* demonstrated that a heterometallic hexanuclear cyanide-bridged complex can undergo reversible structural switching through a concerted rearrangement of coordination and hydrogen bonds, accompanied by a ligand exchange of cyanides.[6] Among other strategies that have recently attracted attention, Costa *et al.* reported a vapochromic system in which the exposure of an Fe(II)-based CP to pyridine vapor induces a stepwise single-crystal-to-single-crystal (SCSC) transformation across 0D, 1D, and 2D structures.[7] However, achieving a reversible transformation between the 0D and 1D forms *via* a simple and practical method remains a significant challenge.[8] This is because 1D CPs, once formed, tend to be structurally robust, making their breakdown into reusable 0D complexes difficult. In addition, exposing single crystals to external stimuli often leads to a loss of crystallinity, preventing SCSC transformations from being controlled.[9]

We focused on copper(I) halide (CuX, X = Cl, Br, or I) complexes as promising candidates for processable and recyclable luminescent CPs. The structural diversity of CuX complexes arises from the formation of various Cu–X clusters, including dinuclear rhombic, tetranuclear cubic, and polymeric ladder architectures.[10] These clusters exhibit characteristic phosphorescence *via* cluster-centered (CC) d–p electronic transitions, whereas mononuclear CuX complexes primarily display luminescence originating from metal-to-ligand charge transfer (MLCT) and/or intraligand π–π^* transitions.[11] Given their unique photophysical properties, CuX clusters can serve as secondary building units (SBUs) for luminescent CPs. Moreover, the flexible and labile nature of Cu···ligand coordination bonds allows for stimuli-responsive structural transformations, which are often accompanied by changes in luminescent properties, making CuX-based materials excellent candidates for smart materials applications.[12] Several studies have explored the processability of CuX-based CPs using transformations between discrete 0D and CP forms. However, to date, no studies have reported luminescent CPs incorporating CuX clusters as SBUs that are capable of reversible interconversion between the 0D and CP forms, which helps achieve both processability and recyclability.

Recently, we reported 1D CPs composed of dinuclear rhombic CuX (X = Br, I) SBU with triphenylarsine ($AsPh_3$) and bidentate N-heteroaromatic linking ligands (**L**), named $[Cu_2I_2(AsPh_3)_2(\mathbf{L})]_n$.[13] These 1D CPs demonstrate intense luminescence compared with 0D $Cu_2I_2(AsPh_3)_2$-based complexes with monodentate N-heteroaromatic ligands. In this study, we found that adding excess 2-methylpyrazine (**meprz**) to 1D CP $[Cu_2I_2(AsPh_3)_2(\mathbf{meprz})]_n$ produced the discrete 0D complex $Cu_2I_2(AsPh_3)_2(\mathbf{meprz})_2$. Interestingly, the $Cu_2I_2(AsPh_3)_2(\mathbf{meprz})_2$ (**Crys-A**) crystal was readily transformed into the $[Cu_2I_2(AsPh_3)_2(\mathbf{meprz})]_n$ (**Crys-B**) crystal by exposure to solvent vapor. In addition, **Crys-A** was recovered upon exposure to **meprz** vapor. Herein, we investigated the structural interconversion between the 0D and 1D forms and demonstrated the processing and recycling of intensely luminescent CP. This is the first example of processable and recyclable luminescent CPs with CuX SBUs employing reversible vapor-induced structural interconversion between 0D and 1D forms.

Results and discussion

The 1D CP $[Cu_2I_2(AsPh_3)_2(\mathbf{meprz})]_n$ (**Crys-B**) was prepared *via* spontaneous evaporation, following a previously reported method (Scheme 1).[13] Single-crystal X-ray diffraction (SC-XRD) analysis revealed that **Crys-B** encapsulated acetonitrile (CH_3CN) molecules as crystallization solvents, with two CH_3CN molecules (7.0 wt%) included per Cu_2I_2 SBU. Thermogravimetric analysis (TGA) further confirmed the solvent content, indicating weight losses of 7.4 wt% in the 90–110 °C range, corresponding to two crystallization solvent molecules per Cu_2I_2 SBU (Fig. S20b). The investigation of the crystal growth conditions for **Crys-B** revealed that the addition of excess **meprz** produced crystals that showed relatively weak luminescence with different colors (green at room temperature) from that of **Crys-B** (yellow at room temperature). SC-XRD analysis revealed that the obtained crystals were composed of the discrete 0D complex $Cu_2I_2(AsPh_3)_2(\mathbf{meprz})_2$ (**Crys-A**). It should be noted that **Crys-A** was obtained by isolating **Crys-B** and subsequently dissolving it in neat **meprz**, rather than by adding excess **meprz** directly to the reaction mixture containing CuI, $AsPh_3$, and CH_3CN. Furthermore, according to the TGA results for **Crys-A**, no inclusions of CH_3CN molecules as crystallization solvents were observed. Instead, the observed weight loss corresponds to the components of the complex, *i.e.*, $AsPh_3$ and **meprz** (Fig. S20a). Notably, when unsubstituted pyrazine was used instead of **meprz**, the transformation could not be induced efficiently because pyrazine is a solid at room temperature and cannot generate sufficient vapor pressure under the experimental conditions.

The structures of **Crys-A** and **Crys-B** [13] were compared using SC-XRD data collected at 93 K (Fig. 2 and Tables S1 and S3). The Cu_2I_2 SBU of **Crys-A** has a dinuclear rhombic cluster, similar to **Crys-B**, and retains the same SBU structure, even when measured at 298 K. The intracluster Cu···Cu distance of **Crys-A** (3.0756(8) Å) is slightly longer than that of **Crys-B** (3.0137(6) Å). Furthermore, the τ_4 values (ideally, tetrahedral:

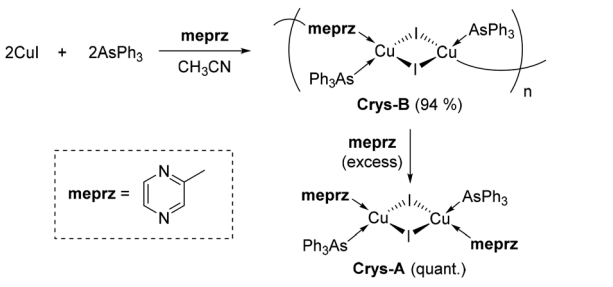

Scheme 1 Synthesis of **Crys-A** and **Crys-B**.

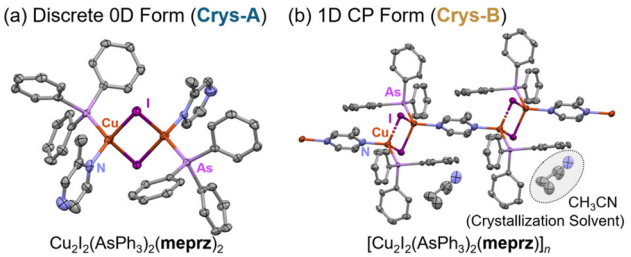

Fig. 2 ORTEP (50% of probability, measured at 93 K) of (a) $Cu_2I_2(AsPh_3)_2$(**meprz**)$_2$ (**Crys-A**) and (b) [$Cu_2I_2(AsPh_3)_2$(**meprz**)]$_n$ (**Crys-B**). Hydrogen atoms are omitted for clarity. Two methyl groups of the **meprz** ligand in **Crys-B** were observed at 50% occupancy each.

τ_4 = 1, square planar: τ_4 = 0),[14] which were calculated based on the bond angles around Cu(I), were 0.904 (**Crys-A**) and 0.912 (**Crys-B**). This suggested that **Crys-A**, formed by the coordination of a new **meprz** ligand to the Cu(I) center in **Crys-B**, exhibited a slight distortion from the ideal tetrahedral geometry. Furthermore, this structural transformation appears to proceed in a manner that compensates for the voids created by the removal of CH_3CN solvent molecules. In **Crys-B**, the methyl group of **meprz** showed positional disorder and was assigned a 50 : 50 occupancy on both sides, indicating that a regio-random polymer structure was adopted. In contrast, in **Crys-A**, the methyl group was oriented toward the Cu(I) center. These observations suggested that the selective formation of the inward-oriented (Cu-directed) conformation of **meprz** was favored during its transformation to **Crys-A**. This is probably because the methyl group sterically blocks the approach of additional free **meprz** molecules from the vapor phase, thereby stabilizing the existing Cu···N coordination and maintaining the dinuclear Cu_2I_2 cluster rather than allowing its dissociation into mononuclear species.

Next, the photoluminescence (PL) properties were evaluated (Fig. 3, S8, S9, S13, and Table S5) to compare the emission maximum (λ_{em}), quantum yield (Φ), and lifetime (τ). At 298 K, **Crys-A** exhibited quite weak green luminescence (λ_{em} = 521 nm, Φ = 0.01), while intense yellow luminescence was observed for **Crys-B** (λ_{em} = 595 nm, Φ = 0.26).[13] This pronounced red shift and higher Φ for **Crys-B** can be discussed in relation to its shorter intracluster Cu···Cu distance and the polymeric structural constraint imposed by the 1D framework. We previously reported the weak emission of the discrete 0D complex $Cu_2I_2(AsPh_3)_2$(2-picoline)$_2$.[15] At 77 K, the emissions of both **Crys-A** and **Crys-B** were red-shifted (λ_{em} = 530 and 629 nm, respectively). In addition, the τ_s turned longer by cooling (**Crys-A:** 0.10 μs (298 K) and 45.6 μs (77 K), **Crys-B:** 4.4 μs (298 K) and 43.5 μs (77 K)[13]). To further clarify the emission mechanism, temperature-dependent PL lifetime measurements of **Crys-B** were performed over a wide temperature range and analyzed using a two-state model considering thermally coupled S_1 and T_1 states (Fig. S19 and Table S9). Arrhenius-type analysis revealed a thermally activated component at elevated temperatures, consistent with reverse intersystem crossing. These results support the assignment of the room-temperature emission to thermally activated delayed fluorescence, whereas the emission at 77 K is dominated by phosphorescence, as commonly observed for rhombic Cu_2I_2 complexes.[13,15,16]

The pronounced differences in the luminescence color and intensity between **Crys-A** and **Crys-B** indicate that the transformation between the 0D and 1D forms can be visually monitored under UV irradiation. To confirm this, structural and luminescent switching were examined using powder X-ray diffraction (PXRD) patterns (Fig. S4) and PL spectra (Table S6 and Fig. S10). First, the powdered **Crys-B** was exposed to **meprz** vapor at 25 °C for 60 min to produce weakly emissive **Crys-A**. Subsequent exposure of **Crys-A** to CH_3CN vapor at 25 °C for 60 min regenerated the strongly emissive **Crys-B**. This interconversion was repeated five times, and PXRD was used to confirm the structural changes (Fig. 4a). The observed PXRD patterns matched those simulated using SC-XRD data. The PL spectra (Fig. 4b) and Φ values (Fig. 4c) were reproducible over five cycles during the interconversion between **Crys-A** and **Crys-B**. It should be noted that when single crystals were subjected to repeated vapor-induced cycles, the transformations

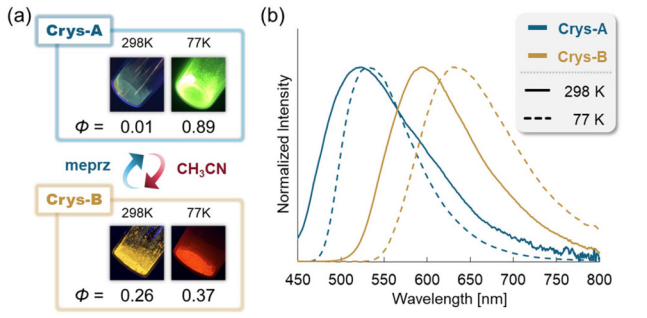

Fig. 3 (a) Photographs with quantum yields (Φ) and (b) PL spectra of **Crys-A** and **Crys-B**, measured at 298 K and 77 K.

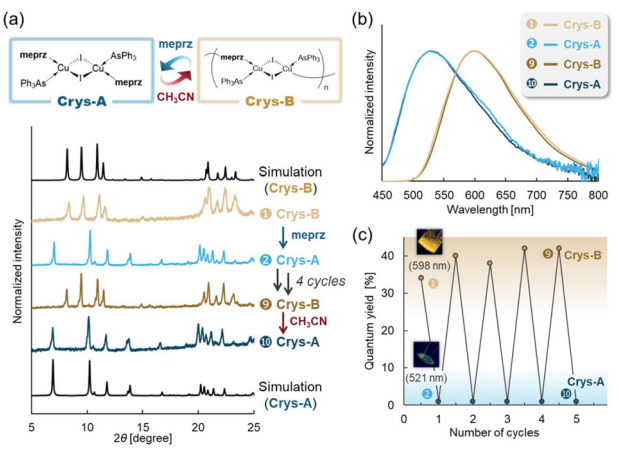

Fig. 4 (a) PXRD patterns (1st, 2nd, 9th, and 10th steps), (b) PL spectra measured at 298 K (1st, 2nd, 9th, and 10th steps), and (c) absolute quantum yields (1st–10th steps) for tracking the vapor-induced interconversion between **Crys-A** and **Crys-B** (vapor exposure: 25 °C, 60 min).

occurred heterogeneously, primarily at or near the crystal surface, resulting in fragmentation and a loss of long-range single-crystal order. As a consequence, reliable SC-XRD data could not be obtained after the vapor-induced cycles, and meaningful comparisons of crystallographic metrics with the pristine structures were not possible. Accordingly, the reversible behavior discussed here is described as a vapor-induced structural interconversion based on powder samples, rather than as a SCSC transition.

For a more detailed insight, time-dependent structural changes were tracked using PXRD in the presence of sodium chloride (NaCl) as an internal standard (Fig. 5). Because the PXRD patterns of **Crys-A** and **Crys-B** exhibit low symmetry and extensive peak overlap, full-profile quantitative analyses such as Rietveld or Le Bail refinement were not applied. Instead, a semi-quantitative analysis based on relative PXRD peak intensities was employed. Powdered **Crys-A** or **Crys-B** (complex: 16.0 mg, NaCl: 4.0 mg) was exposed to CH_3CN or **meprz** vapor. The relative contents of **Crys-A** and **Crys-B** were estimated from the peak intensities at 6.9° (**Crys-A**), 8.3° (**Crys-B**), and 31.9° (NaCl). The transformation from **Crys-A** to **Crys-B** required 60 min, whereas the transformation from **Crys-B** to **Crys-A** was complete within 30 min. These results indicate that ligand elimination and formation of 1D CP require more time than ligand insertion into the 1D framework. Salmon and Routaboul reported that solvent inclusion can accelerate the structural rearrangement in 1D CPs.[17] In the present case, because **Crys-B** contained CH_3CN molecules aligned along the 1D CP chains (Fig. S1b), its transformation to **Crys-A** may have been facilitated, although detailed mechanistic studies are underway. Although no large open channels that allow the free migration of **meprz** molecules are present in the crystal, the incorporated CH_3CN molecules may still assist the structural transformation by promoting local molecular rearrangements. Based on this semi-quantitative analysis, the combined contribution of **Crys-A** and **Crys-B** remained close to unity within the detection limits of laboratory-based PXRD throughout the vapor-induced transformations. No additional diffraction peaks attributable to secondary crystalline phases were observed, and no pronounced increase in diffuse background scattering indicative of significant amorphous content was detected. These observations suggest that the vapor-induced process proceeds predominantly *via* a reversible structural interconversion between **Crys-A** and **Crys-B**.

To further probe the role of solvent vapor in the transformation from **Crys-A** to **Crys-B**, vapor-exposure experiments were conducted using solvents with different polarity and coordinating ability. While methanol, acetone, and toluene vapors did not induce detectable structural changes, dichloromethane vapor led to slow transformations, as confirmed by PXRD (Fig. S5). Among the solvents examined, CH_3CN vapor most efficiently and reproducibly regenerated **Crys-B**, suggesting that small solvent molecules with moderate coordinating ability facilitate the structural interconversion, although the detailed molecular mechanism remains to be elucidated.

We then demonstrated the processing and recycling processes utilizing the transformation between the 0D and 1D forms (Fig. 6). First, **Crys-B** was readily prepared from a CH_3CN solution of CuI, $AsPh_3$, and **meprz** as precipitates (step 1), which were subsequently collected by filtration. **meprz** was then used as a solvent to dissolve **Crys-B**, resulting in a homogeneous solution of $Cu_2I_2(AsPh_3)_2$(**meprz**)$_2$ (step 2). The solution was cast onto a glass substrate, and spin-coating was performed to generate **Crys-A** (step 3); during the drying process, **Crys-A** was partially converted to **Crys-B** considering the luminescence. The exposure to CH_3CN vapor completed the transformation to **Crys-B**, resulting in an intense yellow emission under UV irradiation. The coated film could not be removed using organic solvents because of its CP structure. However, upon exposure to **meprz** vapor, it was transformed

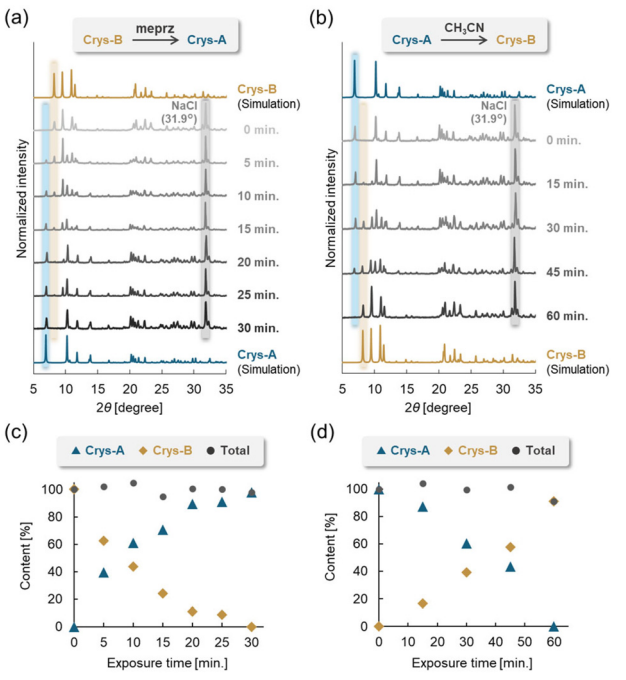

Fig. 5 Time-dependent PXRD patterns of (a) **Crys-B** and (b) **Crys-A** during the exposure to **meprz** and CH_3CN vapor, respectively, in the presence of NaCl. Conversions of (c) **Crys-B** to **Crys-A** and (d) **Crys-A** to **Crys-B**, determined using intensities of the peaks at 6.9° (**Crys-A**), 8.3° (**Crys-B**), and 31.9° (NaCl: internal standard).

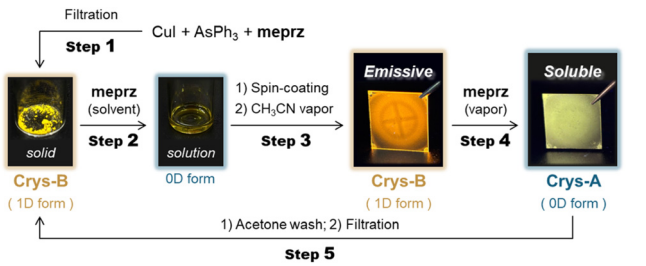

Fig. 6 Demonstration of film fabrication and recycling of the luminescent CuI complex. The photographs of the glass substrates were taken under UV irradiation (365 nm).

into **Crys-A**, the discrete 0D form (step 4), and thereby became readily soluble in common organic solvents such as acetone. In solution, **Crys-B** gradually formed and precipitated, allowing easy collection as return to the initial state (step 5) through the transformation of $Cu_2I_2(AsPh_3)_2$(**meprz**)$_2$ to $[Cu_2I_2(AsPh_3)_2$(**meprz**)$]_n$ *via* the removal of **meprz**. The recovered **Crys-B** sample could be reused to prepare a **meprz** solution of $Cu_2I_2(AsPh_3)_2$(**meprz**)$_2$, indicating that processing and recycling were successful.

Our next focus was the corresponding phosphorus analog to evaluate the effect of replacing $AsPh_3$ with triphenylphosphine (PPh_3). Li *et al.* previously reported the synthesis and photophysical properties of the 1D CP $[Cu_2I_2(PPh_3)_2$(**meprz**)$]_n$ (**Crys-B′**).[12b] However, its transformation behavior has not been investigated. In this work, we succeeded in determining the structure of the discrete 0D complex $Cu_2I_2(PPh_3)_2$(**meprz**)$_2$ (**Crys-A′**) *via* SC-XRD analysis (Tables S2 and S4) and confirmed that its PXRD pattern closely resembled that of the $AsPh_3$-containing 0D complex **Crys-A** (Fig. S3 and S7a). Vapor-induced transformations of the PPh_3 complexes were monitored by PXRD (Fig. 7 and S7), revealing slower conversion rates than those of the $AsPh_3$ analogs. The transformation from **Crys-B′** to **Crys-A′** required 60 min, whereas that from **Crys-A′** to **Crys-B′** required 90 min. In comparison, the transformations of the $AsPh_3$ system were completed within 30 min (from **Crys-B** to **Crys-A**) and 60 min (from **Crys-A** to **Crys-B**), as described above. These findings demonstrate that $AsPh_3$ accelerates vapor-induced structural transformations compared to the conventional phosphorus ligand, PPh_3.

The PL properties of **Crys-A′** and **Crys-B′** were then measured at both 298 K and 77 K, as summarized in Tables S7 and S8. At 298 K, **Crys-A′** and **Crys-B′** showed green (λ_{em} = 547 nm) and orange emissions (λ_{em} = 610 nm), respectively. In stark contrast to the $AsPh_3$ complexes, the Φ_s of **Crys-A′** and **Crys-B′** at 298 K were similar (0.31 and 0.28, respectively). The simultaneous presence of turn-on/off and wavelength-shift response is highly desirable in luminescent sensors; thus, the $AsPh_3$-based system offers advantages in addition to the relatively rapid transformations mentioned above.

Finally, density functional theory (DFT) calculations were performed to gain insights into the reaction mechanism underlying the structural transformation. Particular attention was paid to the difference between the $AsPh_3$ and PPh_3 ligands. Furthermore, the transformation from the 1D CPs (**Crys-B** and **Crys-B′**) to the 0D complexes (**Crys-A** and **Crys-A′**) driven by **meprz** vapor could be successfully analyzed, whereas the reverse transformation could not be elucidated owing to the unclear role of CH_3CN. Dispersion-corrected DFT calculations were performed using the PBE functional with D3 dispersion correction (PBE-D3), implemented in the Vienna *Ab Initio* Simulation Package (VASP, v.6.5.0). The detailed reaction mechanism obtained from the calculations is schematically illustrated in Fig. 8a, and the corresponding optimized structures are shown in Fig. S25. The transformation was initiated by incorporating a **meprz** molecule into the tetrahedrally coordinated Cu(I) center within the Cu_2I_2 SBU of **Crys-B**. Subsequently, ligand addition between the inserted and bridging **meprz** ligands in **Crys-B** cleaved the 1D CP chain, leading to the formation of **Crys-A**. The initial step involved weak binding of **meprz** to **Crys-B** through dispersion interactions, forming an initial complex. The **meprz** ligand then attacked the tetrahedral Cu(I) center *via* a transition state (TS), in which

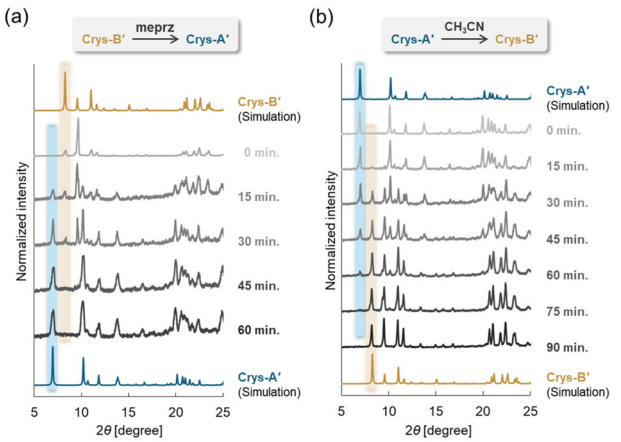

Fig. 7 Time-dependent PXRD patterns of (a) **Crys-B′** and (b) **Crys-A′** during the exposure to **meprz** and CH_3CN vapor, respectively.

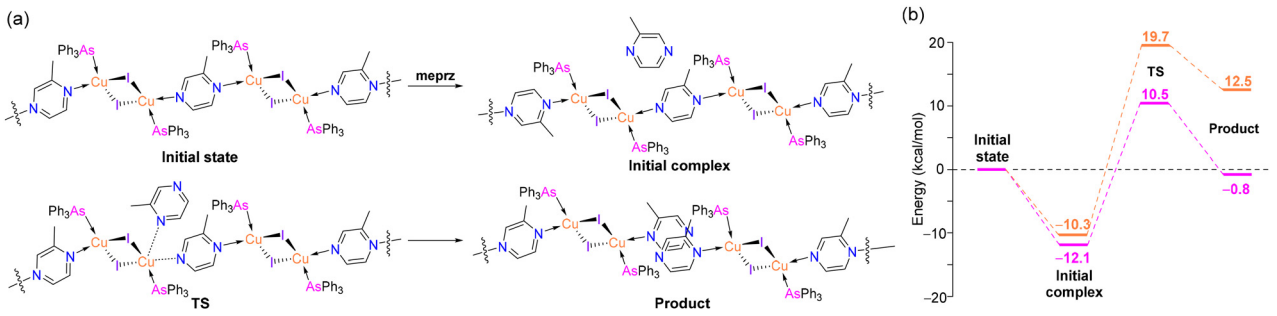

Fig. 8 (a) A proposed mechanism in the ligand addition reaction as the initial step of the transformation from **Crys-B** to **Crys-A**. (b) Potential energy surface in the ligand addition reaction as the initial step of the transformation from **Crys-B** to **Crys-A** (pink line), and that in the phosphorous analog (orange line).

the Cu(I) atom adopted a five-coordinate environment. This high-energy configuration relaxed as the bridging **meprz** dissociated from the Cu(I) center, while a new Cu–N coordination bond was formed simultaneously with the attacking **meprz**. Owing to this ligand addition, the 1D CP chain of **Crys-B** was cleaved, affording the 0D product in which two **meprz** ligands bound to the Cu(I) center stack through π–π interactions. The same transformation occurred at the other Cu(I) center of the Cu_2I_2 SBU, completing the formation of a 0D **Crys-A** structure.

The potential energy surface (PES) for the ligand addition reaction at the Cu(I) center of the Cu_2I_2 SBU in **Crys-B** is shown in Fig. 8b. For comparison, the corresponding reaction in the transformation from **Crys-B′** to **Crys-A′** was also examined (see optimized geometries in Fig. S26). The product of the ligand addition in **Crys-B** lies only −0.8 kcal mol^{-1} relative to the initial state, corresponding to the dissociation limit toward **Crys-B** and **meprz**, whereas that in **Crys-B′** is 12.5 kcal mol^{-1} higher, indicating an endothermic process for the PPh_3 system. More importantly, the transition-state energy for the ligand addition in **Crys-B** was 9.2 kcal mol^{-1} lower than that in **Crys-B′**. This difference is likely attributable to the longer Cu–As bond in the TS (2.34 Å) relative to the Cu–P bond (2.23 Å), which reduces steric repulsion among the surrounding ligands. These results demonstrate that the arsenic ligand $AsPh_3$ facilitates the transformation from the 1D CP to the 0D complex more efficiently than its phosphorus analog PPh_3, which is consistent with the experimental observations.

Conclusions

We have demonstrated a reversible vapor-induced structural interconversion between a zero-dimensional (0D) discrete complex and a one-dimensional (1D) luminescent coordination polymer (CP), both constructed from a triphenylarsine ($AsPh_3$)-coordinated rhombic Cu_2I_2 SBU and 2-methylpyrazine (**meprz**) ligands. The 1D CP $[Cu_2I_2(AsPh_3)_2(\mathbf{meprz})]_n$ (**Crys-B**), which exhibited intense yellow emission, was readily converted into the 0D complex $Cu_2I_2(AsPh_3)_2(\mathbf{meprz})_2$ (**Crys-A**), which was significantly less emissive upon exposure to excess **meprz**. Remarkably, both forward and reverse transformations were achieved under mild conditions using **meprz** and CH_3CN vapors, respectively.

This simple and efficient interconversion process enables solution processing and recycling of luminescent CP, which is an important advancement considering the typically poor processability of CPs owing to their infinite and insoluble frameworks. We demonstrated that **Crys-B** could be deposited on a glass substrate *via* solution casting of **Crys-A**, followed by vapor-induced polymerization and subsequent recovery by vapor-triggered depolymerization. These findings establish a practical approach for processable and recyclable luminescent CPs based on Cu(I) halide clusters.

In addition, experimental and computational studies have revealed that the arsine ligand ($AsPh_3$) promotes faster vapor-induced transformations than its phosphine analog (PPh_3), offering a design strategy for tuning the responsiveness of such systems. Notably, the $AsPh_3$-based complexes exhibit both a pronounced change in emission intensity and a distinct emission color shift between the 0D and 1D forms, which are desirable features for luminescence-based sensing and switching applications.

Overall, our results represent the first example of a CuX-based luminescent CP exhibiting reversible vapor-induced structural interconversion between the 0D and 1D forms, thereby achieving both processability and recyclability. Future studies will focus on extending this concept to other arsine-ligated systems to explore their potential as stimuli-responsive luminescent materials.

Experimental

Materials

Triphenylarsine ($AsPh_3$) was purchased from Sigma-Aldrich (Hattiesburg, Mississippi, US). Acetonitrile (CH_3CN) was purchased from Nacalai Tesque (Kyoto, Japan). Copper(I) iodide (CuI) and 2-methylpyrazine (**meprz**), and triphenylphosphine (PPh_3) were purchased from Wako Pure Chemical Industry (Osaka, Japan). All these reagents were used as commercially available without further purification, and the solvents were used as is. All operations were conducted in air.

1D-CP $[Cu_2I_2(AsPh_3)_2(\mathbf{meprz})]_n$ (**Crys-B**) was synthesized according to a previously reported method.[13]

Measurement

Powder X-ray diffractometry (PXRD) studies were performed on a Rigaku MiniFlex600-C X-ray diffractometer with Cu K_α radiation in the $2\theta/\theta$ mode, and the 2θ scan data were collected at 0.01° intervals and the scan speed was 10° (2θ) min^{-1}. Emission and excitation spectra were obtained on an FP-8500 (JASCO) spectrometer and the absolute PL quantum yields (Φ) were determined by using a JASCO ILFC-847S; the quantum yield of quinine sulfate as reference was 0.52, which is in agreement with the literature value.[18] Emission lifetimes were measured by using a Quantaurus-Tau (Hamamatsu Photonics, Shizuoka, Japan) instrument. Temperature-dependent photoluminescence lifetimes were measured using a Horiba DeltaFlex spectrofluorometer system with an Oxford Optistat DN cryostat for temperature control, and excitation was performed at 375 nm using a diode laser (DeltaDiode DD-375L). Thermogravimetric analysis (TGA) was performed using a Shimadzu DTG-60 thermogravimetric analyzer (Shimadzu, Kyoto, Japan) at a heating rate of 10 °C min^{-1} under N_2 flow.

X-ray crystallographic data for single crystalline products

The single crystal was mounted on a glass fiber. Intensity data were collected at 298 K and 93 K on a Rigaku XtaLAB mini with graphite-monochromated Mo K_α radiation. The readout was performed in the 0.073 mm pixel mode. The data were collected to a maximum 2θ value of 56.8°. Peak finding, indexing, integration, and correction were conducted on CrysAlis^{Pro}.[19]

An analytical numeric absorption correction[20] was applied. The data were corrected for Lorentz and polarization effects. The structure was solved by the direct methods[21] and ShelXT,[22] and was expanded by using Fourier techniques. All refinements were performed on the Olex2[23] crystallographic software package using SHELXL2018 refinement program.[24] Non-hydrogen atoms were refined anisotropically. Hydrogen atoms were refined by using the riding model. The final cycle of the full-matrix least-squares refinement on F^2 was based on observed reflections and variable parameters. Reliability factors are defined as $R_1 = \sum||F_o| - |F_c||/\sum|F_o|(F_o > 2\sigma(F_o))$, $wR_2 = [\sum w(F_o^2 - F_c^2)^2/\sum w(F_o^2)^2]^{1/2}$, and $w = [\delta^2(F_o^2)]^{-1}$. Crystal data and more information on the X-ray data collection are summarized in Tables S1–S4.

Deposition Number 2499226 ($Cu_2I_2(AsPh_3)_2$(**meprz**)$_2$, **Crys-A**, 298 K), 2499227 ($Cu_2I_2(AsPh_3)_2$(**meprz**)$_2$, **Crys-A**, 93 K), 2499228 ($Cu_2I_2(PPh_3)_2$(**meprz**)$_2$, **Crys-A′**, 298 K), and 2499229 ($Cu_2I_2(PPh_3)_2$(**meprz**)$_2$, **Crys-A′**, 93 K) contain the supplementary crystallographic data for this paper.

Computational detail

DFT calculations were carried out to investigate the frontier orbitals and the Wiberg bond indices (WBIs). The full geometries were cited from the single crystal X-ray data collected at 93 K. The calculations employed the combination of B3LYP/6-31G(d) for C, H, N and SDD for Cu, I, As by using the Gaussian 16 program package.[25] The frontier orbitals (HOMO and LUMO+1 levels) and the WBIs of the cuprophilic interaction are shown in Fig. S24 and Table S10, respectively. For analyzing the reaction mechanism of the transformation of **Crys-B** to **Crys-A**, dispersion-corrected DFT calculations with PBE functional (PBE-D3) were performed under periodic boundary conditions (PBC), as implemented in the Vienna *Ab Initio* Simulation Package (VASP v.6.5.0) code.[26,27] The ion–electron interaction was described with the projected augmented wave (PAW) method.[28] A plane-wave basis set with a cutoff energy of 500 eV was used. In the PBC calculations, the Brillouin zone sampling was restricted to only the Γ point. Self-consistent field (SCF) energies were converged with a 1×10^{-5} eV tolerance. The optimization processes converged when the maximum forces on all atoms were less than 0.05 eV Å^{-1}. To identify transition states, we employed the climbing-image nudged elastic band (CI-NEB) method,[29] where 4 intermediate images were used.

Synthesis

Synthesis of $Cu_2I_2(AsPh_3)_2$(meprz)$_2$ (Crys-A) by meprz vapor exposure (Route 1). A powder sample of **Crys-B** (10 mg, 8.9 μmol) was placed in a small sample vial and exposed to **meprz** vapor for an hour, resulting in the quantitative formation of **Crys-A** as a white-yellow powder. The PXRD pattern of the obtained powder matched the simulated pattern based on the single crystal structure of **Crys-A** (Fig. S4a).

Preparation of single crystals of Crys-A. To obtain high-quality single crystals of **Crys-A**, isolated **Crys-B** was dissolved in neat **meprz** and subsequently recrystallized by slow evaporation. A small amount of **Crys-B** was dissolved in **meprz** to give a clear yellow solution. After filtration, the solution was allowed to stand in a small vial, affording yellow-green crystals suitable for single-crystal X-ray diffraction analysis. When **Crys-B** was dissolved in a CH_3CN solution containing **meprz**, **Routes 1** and **2** proceeded simultaneously. As a result, selective formation of **Crys-A** was not achieved; instead, **Crys-B** was recovered, or only a small amount of **Crys-A** was obtained as a minor component. Therefore, solution conditions involving CH_3CN did not allow selective conversion to **Crys-A**.

Synthesis of $[Cu_2I_2(AsPh_3)_2$(meprz)$]_n$ (Crys-B) by CH_3CN vapor exposure (Route 2). A powder sample of **Crys-A** (10 mg, 8.5 μmol) was placed in a small sample vial and exposed to CH_3CN vapor for an hour, resulting in the quantitative formation of **Crys-B** as a yellow powder. The PXRD pattern of the obtained powder matched the simulated pattern based on the single crystal structure of **Crys-B** (Fig. S4b).

Synthesis of $[Cu_2I_2(PPh_3)_2$(meprz)$]_n$ (Crys-B′). Under conditions similar to those used for constructing **Crys-B**,[13] a liquid sample of **meprz** co-ligand (0.025 mmol) was sequentially treated with CH_3CN solutions (10.0 mL) of PPh_3 (14.0 mg, 0.05 mmol) and CuI (10.0 mg, 0.05 mmol). After slow evaporation over several days, crystals were collected by filtration: $[Cu_2I_2(PPh_3)_2$(**meprz**)$]_n$ (2 eq. of CH_3CN, orange crystal, 25.6 mg, 94%). The PXRD pattern of the obtained samples matched the simulated pattern based on the CCDC data (CCDC 1510196) of single crystal structures (Fig. S6).

Synthesis of $Cu_2I_2(PPh_3)_2$(meprz)$_2$ (Crys-A′) by meprz vapor exposure (Route 1′). A powder sample of **Crys-B′** (10 mg, 9.6 μmol) was placed in a small sample vial and exposed to **meprz** vapor for an hour, resulting in the quantitative formation of **Crys-A′** as a white-yellow powder. The PXRD pattern of the obtained powder matched the simulated pattern based on the single crystal structure of **Crys-A′** (Fig. S7a).

Preparation of single crystals of Crys-A′. A small amount of **Crys-B′** was dissolved in **meprz** to give a clear yellow solution. After filtration, the solution was allowed to stand in a small vial, affording yellow-green crystals suitable for single-crystal X-ray diffraction analysis.

Synthesis of $[Cu_2I_2(PPh_3)_2$(meprz)$]_n$ (Crys-B′) by CH_3CN vapor exposure (Route 2′). A powder sample of **Crys-A′** (10 mg, 9.1 μmol) was placed in a small sample vial and exposed to CH_3CN vapor for an hour, resulting in the quantitative formation of **Crys-B′** as a yellow powder. The PXRD pattern of the obtained powder matched the simulated pattern based on the single crystal structure of **Crys-B′** (Fig. S7b).

Author contributions

K. Kikuchi: synthesis, structural analysis, data curation, and writing – original draft; S. Nagata: DFT calculations, data curation, and writing – original draft; T. Yumura: DFT calculations, data curation, and writing – original draft; T. Iwamoto: conceptualization, investigation, writing – review and editing, and supervision; K. Naka: conceptualization, investigation, writing

– review and editing, and supervision; H. Imoto: conceptualization, investigation, writing – original draft, writing – review and editing, funding acquisition, project administration, and supervision.

Conflicts of interest

There are no conflicts to declare.

Data availability

The authors confirm that the data supporting the findings of this study are available within the article and its supplementary information (SI). Supplementary information: X-ray diffraction data, photophysical data, TGA data, and computational calculations. See DOI: **https://doi.org/10.1039/d5qi02376a**.

CCDC 2499226–2499229 contain the supplementary crystallographic data for this paper.[30a–d]

Acknowledgements

We thank Prof. Kazuo Tanaka, Prof. Shunichiro Ito, Mr Kazuhiro Yuhara, and Ms Mei Tokutomi of Kyoto University for their assistance with variable-temperature luminescence lifetime measurements. This work was supported by JSPS KAKENHI (grant number 23H02009 [Grant-in-Aid for Scientific Research (B)]) to HI and JST, grant number JPMJFR221K (FOREST Program) to HI, and JPMJFS2124 (the establishment of university fellowships towards the creation of science technology innovation) to KK.

References

1 For reviews, see: (*a*) C. Janiak, Engineering coordination polymers towards applications, *Dalton Trans.*, 2003, 2781–2804; (*b*) K. Biradha, A. Ramanan and J. J. Vittal, Coordination Polymers Versus Metal–Organic Frameworks, *Cryst. Growth Des.*, 2009, **9**, 2969–2970; (*c*) Y. Hasegawa and T. Nakanishi, Luminescent lanthanide coordination polymers for photonic applications, *RSC Adv.*, 2015, **5**, 338–353; (*d*) Y. Hasegawa and Y. Kitagawa, Thermo-sensitive luminescence of lanthanide complexes, clusters, coordination polymers and metal–organic frameworks with organic photosensitizers, *J. Mater. Chem. C*, 2019, **7**, 7494–7511; (*e*) J.-Q. Liu, Z.-D. Luo, Y. Pan, A. K. Singh, M. Trivedi and A. Kumar, Recent developments in luminescent coordination polymers: Designing strategies, sensing application and theoretical evidences, *Coord. Chem. Rev.*, 2020, **406**, 213145; (*f*) G. H. Morritt, H. Michaels and M. Freitag, Coordination polymers for emerging molecular devices, *Chem. Phys. Rev.*, 2022, **3**, 011306.

2 (*a*) K. Miyata, T. Ohba, A. Kobayashi, M. Kato, T. Nakanishi, K. Fushimi and Y. Hasegawa, Thermostable Organo-phosphor: Low-Vibrational Coordination Polymers That Exhibit Different Intermolecular Interactions, *ChemPlusChem*, 2012, **77**, 277–280; (*b*) Y. Hirai, T. Nakanishi and Y. Hasegawa, Organo-lanthanide luminophores bridged by phosphine oxide ligands, *J. Lumin.*, 2016, **170**, 801–807; (*c*) K. Miyata, Y. Konno, T. Nakanishi, A. Kobayashi, M. Kato, K. Fushimi and Y. Hasegawa, Chameleon Luminophore for Sensing Temperatures: Control of Metal-to-Metal and Energy Back Transfer in Lanthanide Coordination Polymers, *Angew. Chem., Int. Ed.*, 2013, **52**, 6413–6416; (*d*) M. Yamamoto, T. Nakanishi, Y. Kitagawa, T. Seki, H. Ito, K. Fushimi and Y. Hasegawa, Synthesis and Photophysical Properties of Eu(III) Complexes with Phosphine Oxide Ligands including Metal Ions, *Bull. Chem. Soc. Jpn.*, 2018, **91**, 6–11; (*e*) Y. Hasegawa and Y. Kitagawa, Luminescent lanthanide coordination polymers with transformative energy transfer processes for physical and chemical sensing applications, *J. Photochem. Photobiol., C*, 2022, **51**, 100485.

3 (*a*) H. B. T. Jeazet, C. Staudt and C. Janiak, Metal–organic frameworks in mixed-matrix membranes for gas separation, *Dalton Trans.*, 2012, **41**, 14003–14027; (*b*) J. Dechnik, J. Gascon, C. J. Doonan, C. Janiak and C. J. Sumby, Mixed-Matrix Membranes, *Angew. Chem., Int. Ed.*, 2017, **56**, 9292–9310; (*c*) B. Ghalei, K. Sakurai, Y. Kinoshita, K. Wakimoto, A. P. Isfahani, Q. Song, K. Doitomi, S. Furukawa, H. Hirao, H. Kusuda, S. Kitagawa and E. Sivaniah, Enhanced selectivity in mixed matrix membranes for CO_2 capture through efficient dispersion of amine-functionalized MOF nanoparticles, *Nat. Energy*, 2017, **2**, 17086.

4 M. Yamada, Synthesis of Organic Shell–Inorganic Core Hybrid Nanoparticles by Wet Process and Investigation of Their Advanced Functions, *Bull. Chem. Soc. Jpn.*, 2009, **82**, 152–170.

5 D. Shen, Y. Jin, Z. Zhang, R. Song, M. Liu, W. Li, X. Li, R. Wu, B. Li, J. Li, B. Zhao and X. Duan, Recent Advances in Spin-coating Precursor Mediated Chemical Vapor Deposition of Two-Dimensional Transition Metal Dichalcogenides, *Precis. Chem.*, 2024, **2**, 282–299.

6 R. Gheorghe, M. Kalisz, R. Clérac, C. Mathonière, P. Herson, Y. Li, M. Seuleiman, R. Lescouëzec, F. Lloret and M. Julve, Dimensionality Switching Through a Thermally Induced Reversible Single-Crystal-to-Single-Crystal Phase Transition in a Cyanide Complex, *Inorg. Chem.*, 2010, **49**, 11045–11056.

7 E. Fernandez-Bartolome, E. Resines-Urien, M. Murillo-Vidal, L. Piñeiro-Lopez and J. S. Costa, Sequential single-crystal-to-single-crystal vapochromic inclusion in a nonporous coordination polymer: unravelling dynamic rearrangement for selective pyridine sensing, *Inorg. Chem. Front.*, 2021, **8**, 2426–2432.

8 M. Deng, S. Mukherjee, Y.-J. Liang, X.-D. Fang, A.-X. Zhu and M. J. Zaworotko, Water vapour induced reversible switching between a 1-D coordination polymer and a 0-D aqua complex, *Chem. Commun.*, 2022, **58**, 8218–8221.

9 (*a*) A. Chaudhary, A. Mohammad and S. M. Mobin, Recent Advances in Single-Crystal-to-Single-Crystal Transformation at the Discrete Molecular Level, *Cryst. Growth Des.*, 2017, **17**, 2893–2910; (*b*) E. Fernandez-Bartolome, A. Martinez-Martinez, E. Resines-Urien, L. Piñeiro-Lopez and J. S. Costa, Reversible single-crystal-to-single-crystal transformations in coordination compounds induced by external stimuli, *Coord. Chem. Rev.*, 2022, **452**, 214281.

10 (*a*) R. Peng, M. Li and D. Li, Copper(I) halides: A versatile family in coordination chemistry and crystal engineering, *Coord. Chem. Rev.*, 2010, **254**, 1–18; (*b*) J. Conesa-Egea, F. Zamora and P. Amo-Ochoa, Perspectives of the smart Cu-Iodine coordination polymers: A portage to the world of new nanomaterials and composites, *Coord. Chem. Rev.*, 2019, **381**, 65–78; (*c*) J. Troyano, F. Zamora and S. Delgado, Copper(I)–iodide cluster structures as functional and processable platform materials, *Chem. Soc. Rev.*, 2021, **50**, 4606–4628; (*d*) A. Forni, D. Malpicci, E. Lucenti, L. Zecchinello, A. Colombo and E. Cariati, Recent advances in mono- and multi-nuclear photoluminescent Cu(I) complexes with nitrogen containing ligands and their stimuli responsiveness, *Chem. Sci.*, 2025, **16**, 20755–20805.

11 (*a*) C. E. A. Palmer and D. R. McMillin, Singlets, triplets, and exciplexes: complex, temperature-dependent emissions from (2,9-dimethyl-1,10-phenanthroline)bis(triphenylphosphine)copper(1+) and (1,10-phenanthroline)(triphenylphosphine)copper(1+), *Inorg. Chem.*, 1987, **26**, 3837–3840; (*b*) P. C. Ford, E. Cariati and J. Bourassa, Photoluminescence Properties of Multinuclear Copper(I) Compounds, *Chem. Rev.*, 1999, **99**, 3625–3648; (*c*) M. Vitale and P. C. Ford, Luminescent mixed ligand copper(I) clusters $(CuI)_n(L)_m$ (L=pyridine, piperidine): thermodynamic control of molecular and supramolecular species, *Coord. Chem. Rev.*, 2001, **219–221**, 3–16; (*d*) A. Tsuboyama, K. Kuge, M. Furugori, S. Okada, M. Hoshino and K. Ueno, Photophysical Properties of Highly Luminescent Copper(I) Halide Complexes Chelated with 1,2-Bis(diphenylphosphino)benzene, *Inorg. Chem.*, 2007, **46**, 1992–2001; (*e*) H. Kitagawa, Y. Ozawa and K. Toriumi, Flexibility of cubane-like Cu_4I_4 framework: temperature dependence of molecular structure and luminescence thermochromism of $[Cu_4I_4(PPh_3)_4]$ in two polymorphic crystalline states, *Chem. Commun.*, 2010, **46**, 6302–6304; (*f*) M. J. Leitl, F.-R. Küchle, H. A. Mayer, L. Wesemann and H. Yersin, Brightly Blue and Green Emitting Cu(I) Dimers for Singlet Harvesting in OLEDs, *J. Phys. Chem. A*, 2013, **117**, 11823–11836.

12 (*a*) W. Liu, Y. Fang, G. Z. Wei, S. J. Teat, K. Xiong, Z. Hu, W. P. Lustig and J. Li, A Family of Highly Efficient CuI-Based Lighting Phosphors Prepared by a Systematic, Bottom-up Synthetic Approach, *J. Am. Chem. Soc.*, 2015, **137**, 9400–9408; (*b*) W. Liu, K. Zhu, S. J. Teat, B. J. Deibert, W. Yuan and J. Li, A mechanochemical route toward the rational, systematic, and cost-effective green synthesis of strongly luminescent copper iodide based hybrid phosphors, *J. Mater. Chem. C*, 2017, **5**, 5962–5969; (*c*) H. Ohara, T. Ogawa, M. Yoshida, A. Kobayashi and M. Kato, Reversible luminescent colour changes of mononuclear copper(I) complexes based on ligand exchange reactions by N-heteroaromatic vapours, *Dalton Trans.*, 2017, **46**, 3755–3760; (*d*) T. Hasegawa, A. Kobayashi, H. Ohara, M. Yoshida and M. Kato, Emission Tuning of Luminescent Copper(I) Complexes by Vapor-Induced Ligand Exchange Reactions, *Inorg. Chem.*, 2017, **56**, 4928–4936; (*e*) S. Kondo, N. Yoshimura, M. Yoshida, A. Kobayashi and M. Kato, Vapochromic luminescence of a spin-coated copper(I) complex thin film by the direct coordination of vapour molecules, *Dalton Trans.*, 2020, **49**, 16946–16953; (*f*) S. Kondo, N. Yoshimura, A. Kobayashi, K. D. C. Kuruppu, W. M. C. Sameera, S. Fujii, M. Yoshida and M. Kato, Vapoluminescent thin-film with unsaturated copper(I) complex for rapid light-on sensing of N-heteroaromatic vapour, *J. Mater. Chem. C*, 2024, **12**, 1799–1808.

13 K. Kikuchi, H. Imoto and K. Naka, Robust and highly emissive copper(I) halide 1D-coordination polymers with triphenylarsine and a series of bridging N-heteroaromatic co-ligands, *Dalton Trans.*, 2023, **52**, 11168–11175.

14 L. Yang, D. R. Powell and R. P. Houser, Structural variation in copper(I) complexes with pyridylmethylamide ligands: structural analysis with a new four-coordinate geometry index, τ_4, *Dalton Trans.*, 2007, 955–964.

15 R. Kobayashi, H. Imoto and K. Naka, Stimuli-Responsive Emission of Dinuclear Rhombic Copper(I) Iodide Complexes Having Triphenylarsine and N-Heteroaromatic Co-Ligands, *Eur. J. Inorg. Chem.*, 2020, **2020**, 3548–3553.

16 Y. V. Demyanov, M. I. Rakhmanova, I. Y. Bagryanskaya and A. V. Artem'ev, 1D CuI coordination polymers based on triphenylarsine and *N*,*N*'-ditopic co-ligands: synthesis, crystal structure and TADF properties, *Mendeleev Commun.*, 2022, **32**, 649–651.

17 A. Enríquez-Cabrera, L. Getzner, L. Salmon, L. Routaboul and A. Bousseksou, Post-synthetic modification mechanism for 1D spin crossover coordination polymers, *New J. Chem.*, 2022, **46**, 22004–22012.

18 K. Kinoshita and K. Mihashi, *Fluorescence Measurements, Application to Bioscience, Measurement Method, Series 3*, Spectroscopical Society of Japan, Academic Publication Center, 1983.

19 *CrysAlisPro, Data Collection and Processing Software*, Rigaku Oxford Diffraction, Tokyo 196-8666, Japan, 2020.

20 R. C. Clark and J. S. Reid, The analytical calculation of absorption in multifaceted crystals, *Acta Crystallogr., Sect. A: Found. Crystallogr.*, 1995, **51**, 887–897.

21 SIR2011; M. C. Burla, R. Caliandro, M. Camalli, B. Carrozzini, G. L. Cascarano, C. Giacovazzo, M. Mallamo, A. Mazzone, G. Polidori and R. Spagna, *SIR2011*: a new package for crystal structure determination and refinement, *J. Appl. Crystallogr.*, 2012, **45**, 357–361.

22 SHELXT; G. M. Sheldrick, Crystal structure refinement with *SHELXL*, *Acta Crystallogr., Sect. C: Struct. Chem.*, 2015, **71**, 3–8.

23 Olex2; O. V. Dolomanov, L. J. Bourhis, R. J. Gildea, J. A. K. Howard and H. Puschmann, *OLEX2*: a complete

structure solution, refinement and analysis program, *J. Appl. Crystallogr.*, 2009, **42**, 339–341.

24 SHELXL2018; G. M. Sheldrick, *SHELXL-2018/3, Program for the Refinement of Crystal Structures*, University of Goettingen, Goettingen, Germany, 2018.

25 M. J. Frisch, G. W. Trucks, H. B. Schlegel, G. E. Scuseria, M. A. Robb, J. R. Cheeseman, G. Scalmani, V. Barone, G. A. Petersson, H. Nakatsuji, X. Li, M. Caricato, A. V. Marenich, J. Bloino, B. G. Janesko, R. Gomperts, B. Mennucci, H. P. Hratchian, J. V. Ortiz, A. F. Izmaylov, J. L. Sonnenberg, D. Williams-Young, F. Ding, F. Lipparini, F. Egidi, J. Goings, B. Peng, A. Petrone, T. Henderson, D. Ranasinghe, V. G. Zakrzewski, J. Gao, N. Rega, G. Zheng, W. Liang, M. Hada, M. Ehara, K. Toyota, R. Fukuda, J. Hasegawa, M. Ishida, T. Nakajima, Y. Honda, O. Kitao, H. Nakai, T. Vreven, K. Throssell, J. A. Montgomery Jr., J. E. Peralta, F. Ogliaro, M. J. Bearpark, J. J. Heyd, E. N. Brothers, K. N. Kudin, V. N. Staroverov, T. A. Keith, R. Kobayashi, J. Normand, K. Raghavachari, A. P. Rendell, J. C. Burant, S. S. Iyengar, J. Tomasi, M. Cossi, J. M. Millam, M. Klene, C. Adamo, R. Cammi, J. W. Ochterski, R. L. Martin, K. Morokuma, O. Farkas, J. B. Foresman and D. J. Fox, *Gaussian 16, Revision C.01*, Gaussian, Inc., Wallingford CT, 2016.

26 J. Furthmüller, J. Hafner and G. Kresse, *Ab initio* calculation of the structural and electronic properties of carbon and boron nitride using ultrasoft pseudopotentials, *Phys. Rev. B: Condens. Matter Mater. Phys.*, 1994, **50**, 15606.

27 G. Kresse and J. Furthmüller, Efficiency of *ab initio* total energy calculations for metals and semiconductors using a plane-wave basis set, *Comput. Mater. Sci.*, 1996, **6**, 15–50.

28 P. E. Blöchl, Projector augmented-wave method, *Phys. Rev. B: Condens. Matter Mater. Phys.*, 1994, **50**, 17953.

29 G. Henkelman, B. P. Uberuaga and H. Jónsson, A climbing image nudged elastic band method for finding saddle points and minimum energy paths, *J. Chem. Phys.*, 2000, **113**, 9901–9904.

30 (*a*) CCDC 2499226: Experimental Crystal Structure Determination, 2026, DOI: **10.5517/ccdc.csd.cc2pwn6g**; (*b*) CCDC 2499227: Experimental Crystal Structure Determination, 2026, DOI: **10.5517/ccdc.csd.cc2pwn7h**; (*c*) CCDC 2499228: Experimental Crystal Structure Determination, 2026, DOI: **10.5517/ccdc.csd.cc2pwn8j**; (*d*) CCDC 2499229: Experimental Crystal Structure Determination, 2026, DOI: **10.5517/ccdc.csd.cc2pwn9k**.

